Evaluation of compressive membrane action effects on punching shear resistance of reinforced concrete slabs

EVALUATION OF COMPRESSIVE MEMBRANE ACTION EFFECTS ON PUNCHING SHEAR RESISTANCE OF REINFORCED CONCRETE SLABS

Beatrice Belletti[a], Joost Walraven[b], Francesco Trapani[a]

[a] *DICATeA, University of Parma, Parco Area delle Scienze, 181/a, 43124 Parma, Italy, beatrice.belletti@unipr.it*

[b] *Department Design and Construction, Delft, University of Technology, Stevinweg 1, 2628 CN, Delft, the Netherlands*

Abstract

It is widely recognized that Compressive Membrane Action (CMA), also called Arching Action, increases both the bending and punching capacities of reinforced concrete (RC) structures. In this paper a non-linear finite element (NLFE) approach which adopts multi-layered shell modelling of RC slabs is presented. NLFE analyses (NLFEA) were carried out with ABAQUS Code and UMAT.for user subroutine in which the crack model denoted as Physical Approach for Reinforced Concrete for Cyclic Loading (PARC_CL) was implemented. Post-processing of NLFEA results is presented which exploits the Critical Shear Crack Theory (CSCT) to evaluate the punching shear resistance of shell elements. The capability of the proposed numerical procedure, to properly determine the punching shear resistance of RC slabs, is checked by comparing numerical predictions with experimental punching shear capacities obtained on circular slabs tested at the Stevin Laboratory of TU Delft. Subsequently the same numerical procedure was adopted to evaluate CMA effects on the punching shear resistance of the Corick bridge deck in Ireland, UK, subjected to concentrated loads. Finally the design punching shear resistances achieved with the presented procedure are compared with the analytical values obtained using the British Code BD81/02.

1 Introduction

Arching Action can develop when the edges of the loaded member are restrained against lateral displacements; when the edges of the member are prevented from lateral displacement, in-plane compressive thrusts rise from the boundary enhancing the load-carrying capacity, Figure 1.

CMA effects can be regarded in the analysis of the behavior of bridge deck slabs [1], [2], slab to column connections, offshore concrete structures [3], underground structures subjected to earth pressure, slabs subjected to large displacement due to fire [4] and slabs subjected to a sudden removal of a supporting column [5]. It has been demonstrated that CMA acts, with lower effects, also in the case of unrestrained slabs [6].

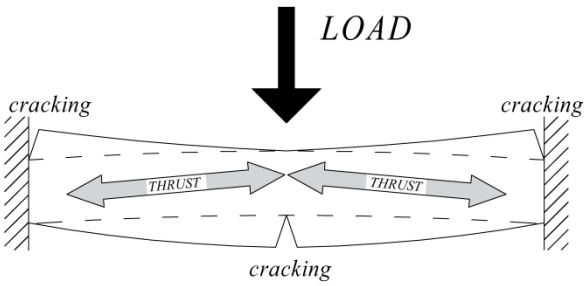

Figure 1 - Compressive membrane action in laterally restrained slab.

In the last fifty years several experimental programs have been developed to investigate CMA effects but, due to the complexity of the problem, nowadays this phenomenon is considered only by a few Codes (Canadian [7], British [2] and New Zealand [8] Codes) keeping this effect unknown for many practicing engineers which adopt more conservative flexural theories.

Most of the research devoted to the study of CMA effects aims at demonstrating the improvement of the bearing capacity of the slab caused by this effect ([9] - [11]). The dependency of both geometrical and mechanical parameters on the enhancement of RC slab bearing capacity due to CMA effects, has been investigated during the years by varying the specimen boundary conditions ([12] - [14]), the slab thickness and reinforcement [15], the compressive strength of concrete [16] and the percentage of fibres for fibre-reinforced concrete (FRC), [1], [17]. Experiments on post-tensioned bridge deck slabs have been recently carried out at the Stevin Laboratory of TU Delft to include CMA effects in the punching shear assessment of prestressed bridge deck slabs [18]-[19].

However, the utmost part of the studies on CMA effects refers to RC bridge deck slabs ([17]-[20]). Indeed, considering CMA effects in the re-assessment of the carrying capacity of existing structures, leads sometimes to satisfying the defined performance requirements by virtue of mobilizing residual bearing capacity and to avoiding any expensive retrofitting.

Over the years the formulation of analytical relations incorporating CMA effects has been an important challenge for researchers. Since the 80's several researchers recognized that the definition of lateral restraining stiffness and strength provided by boundary conditions is fundamental to develop proper theories on arching action for RC slabs [21]. In the 70's several tests [22]-[23], sponsored by the Ontario Ministry of Transportation, led to empirical design specifications taking into account CMA in the Ontario Highway Bridge Design Code [24].

In the UK, Rankin and Long [25] developed an elastic-plastic deformation method for predicting the arching action strength enhancement in laterally restrained one-way slab strips. Some virtual work based methods have also been formulated for the capacity assessment of two-way RC slabs using strip methods [3], [26]. A detailed procedure to calculate the effects of CMA has been provided by Das and Morley [27] for the particular case of circular slabs.

In 2002, based on the work of Kirkpatrick et al. [28] and Rankin and Long [25], the British Code [2] provided formulations for the assessment of RC slab capacity which included an additional percentage of flexural reinforcement equivalent to CMA effects.

The difficulties encountered in the definition of the boundary conditions, for the application of analytical formulations, led to the use of NLFE methods for the evaluation of the flexural and shear resistance of RC slabs modelled with brick [19],[29], [30] or shell [31], [32] elements.

In this paper a NLFE approach which adopts multi-layered shell modelling of RC slabs is presented. Over their thickness the shell elements are subdivided in layers whose non-linear behavior is described by the PARC_CL crack model [33]. The same approach has been applied in the previous works for the prediction of the crack pattern development and bending failure mode of RC slabs tested by Taylor [34] having different reinforcement arrangements [35]; for the design of steel fiber-reinforced concrete pavements [36]; for the assessment of the bearing capacity of precast roof elements characterized by geometric and mechanical non-linearity [37] and for pushover analyses of RC structural wall systems [38]. Since shell elements do not include the non-linear behavior due to shear along the thickness of the shell, in this paper post-processing of the NLFEA results is conducted based on the Critical Shear Crack Theory (CSCT) presented in [39]. Several applications of the Critical Shear Crack Theory can be found in literature for the evaluation of the shear punching resistance by FEM [29], [40] or sector based methods [41]. Model Code 2010 [42] adopts the CSCT failure criterion combined with the Levels of Approximation (LoA) approach. This approach is based on the use of different methods depending on the degree of accuracy desired, from LoA I to LoA IV. In this paper LoA IV is adopted for the evaluation of the rotation of slabs by using NLFE analyses.

In the first part of the paper a comparison between NLFEA results and experimental observations on circular slabs tested at the Stevin Laboratory of TuDelft [12] are presented to verify that the proposed procedure is able to properly evaluate the punching shear resistance of confined and un-confined reinforced concrete (RC) and steel fibre reinforced concrete (SFRC) slabs.

In the second part of the paper the same numerical procedure is adopted to predict CMA effects in the structural response of the Corick bridge, subjected to concentrated loads, experimentally investigated by Taylor et al. [1].

Finally the design punching shear resistances achieved by combining the multi-layered shell modelling and the PARC_CL crack model with the CSCT failure criterion are compared with the values obtained with the British Code BD81/02 [2]. The design punching shear resistance is calculated by adopting the Method of Estimation of the Coefficient of Variation of resistance (ECOV) which is one of the alternative safety format methods proposed in the Model Code 2010 [42] for the structural verification assisted by numerical simulation.

2 Multi-layered shell element modelling and PARC_CL crack model

Multi-layered shell modelling and the PARC_CL crack model can predict the non-linear behavior of RC slabs subjected to bending moments and/or axial forces very well, but is unable to predict the non-linear behavior due to shear through the slab thickness. For members subjected to concentrated loads, the punching shear resistance can be properly evaluated with brick elements or axisymmetric elements if appropriate crack models and modelling strategies are adopted. However, for the evaluation of both global and local failure modes, finite element models of real structures cannot easily be carried out with the previously mentioned modeling. Indeed due to several load combinations of actions that have to be considered in the design verification process, NLFE modelling adopting brick elements requires a lot of time and memory space for the analyses.

In order to develop a general procedure for the prediction of both the flexural and the shear resistance through a NLFE method, multi-layered shell elements seem to be a suitable choice. Indeed, memory space and time requirement for NLFE analyses involved in shell element modeling is much less than needed when using brick elements. In this paper the punching shear capacity is evaluated through a post processing method by adopting the Critical Shear Crack Theory which enables the punching shear resistance evaluation as a function of the rotation of the slab. The relation between the applied load and the rotation of the slab is obtained from NLFE analyses carried out using the PARC_CL model implemented in the user subroutine UMAT.for of the ABAQUS Code.

2.1 Multi-layered shell element modelling

Both geometric and mechanical non-linearities have been taken into account. Mechanical non-linearity is evaluated using the PARC_CL crack model while geometric non-linearity has been considered by adopting an updated Lagrangian formulation.

2.2 PARC_CL Crack Model

The PARC_CL model is a constitutive model for the analysis of the non-linear behavior up to failure of reinforced concrete membrane elements [33]. The PARC_CL model is an extension of the crack model called Physical Approach for Reinforced Concrete (PARC) implemented for monotonic loading [43]. The thickness of shell elements is subdivided in layers subjected to plane stresses, Figure 2(a). The element is reinforced with i rebars placed along the x_i-axis, forming an angle θ_i with the local element x-axis, and having a steel reinforcement ratio ρ_i, Figure 2(b). The pattern of the cracks, occurring when the principal stress reaches the tensile strength of the concrete f_{ct}, is assumed to maintain a fixed orientation upon further loading; the distance between the cracks a_m is assumed to be constant and it is determined by an ‘‘a priori’’ according to the formulation given in Eq.(1):

$$a_m = \left(\frac{\cos\alpha}{\ell_{sx}} + \frac{\sin\alpha}{\ell_{sy}} \right)^{-1} \tag{1}$$

being α the angle formed between x_i-axis and *1*-axis and ℓ_{sx} and ℓ_{sy} the slip lengths in the two orthogonal directions evaluated according to Model Code 2010 [42] formulations.

The main parameters that govern the problem are the crack width *w*, the crack slip *v* and the strut concrete strain between the cracks ε_2, see Figure 2. Both in the uncracked phase and in the cracked phase the total stiffness matrix is obtained by adding the contributions of concrete and steel, which are considered as two springs acting in parallel. The nonlinear mechanical behavior is described by the constitutive laws of the structural materials and by the interface mechanisms (tension stiffening, dowel action, aggregate interlock). For further details reference is made to [33] and [43].

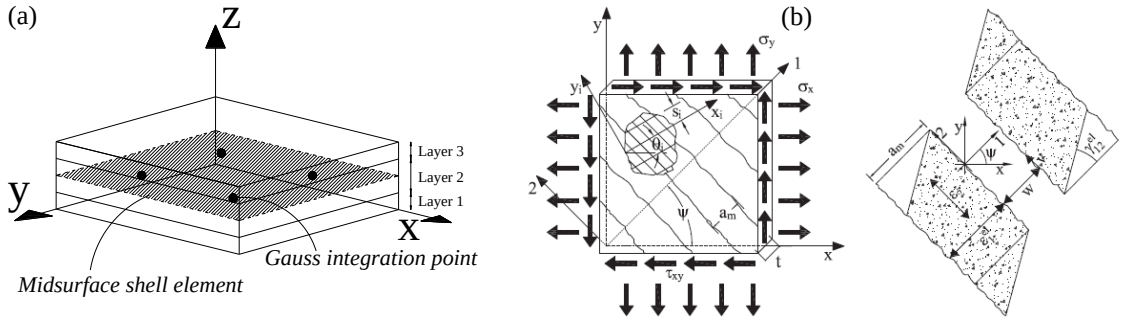

Figure 2 - a) Multi-layered shell element; (b) Reinforced concrete membrane element subjected to a plane stress state: displacement and deformation parameters involved in PARC_CL crack model.

2.3 Critical Shear Crack Theory

To predict the punching shear resistance of a slab subjected to a concentrated load with multi-layered shell elements and the PARC_CL crack model, post-processing of NLFEA results is proposed in this paper according to the Critical Shear Crack Theory [39]. The CSCT theory states that the punching shear resistance (V_R) depends on the crack width (w) and the roughness of the critical shear crack developing from the loaded area into the slab, Figure 3.

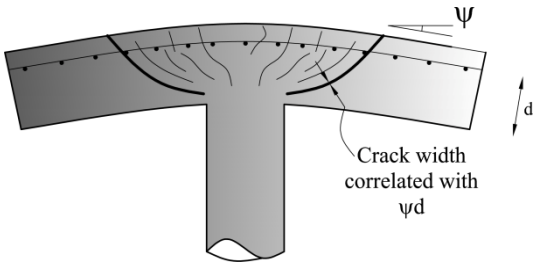

Figure 3 - Critical inclined crack developing from the loaded area into the slab.

The failure criterion, expressed by Eq.(2) was proposed by Muttoni [39] assuming that the critical shear crack width, *w*, is proportional to the product of the slab rotation (ψ), which is the rotation of the slab around the load introduction area, and the average effective depth (*d*) of the slab, Figure 3.

Eq.(2) was formulated assuming that the roughness of the crack is correlated to the maximum aggregate size (d_g):

$$V_R(\psi) = \frac{3/4 \cdot b_0 \cdot d_v \sqrt{f_c}}{1+15\dfrac{\psi \cdot d}{d_g + d_{g0}}} \tag{2}$$

The idea behind this is that the punching shear capacity depends substantially on the contribution of aggregate interlock across the inclined cracks. The larger is the inclined crack width, the smaller is the contribution of shear friction (aggregate interlock) to the punching shear capacity.

In Eq.(2) $V_R(\psi)$ is the punching shear resistance, b_0 is the length of the control perimeter, located at $d/2$ from the loaded area, d_v is the shear-resisting effective depth and f_c is the average value for the compressive strength of concrete.

Graphically, this equation represents a curve that creates a limit between bending and punching shear failure. Punching shear failure occurs at the intersection between the load-rotation curve of the slab, obtained from NLFEA or analytical methods, and the CSCT failure criterion, Figure 4.

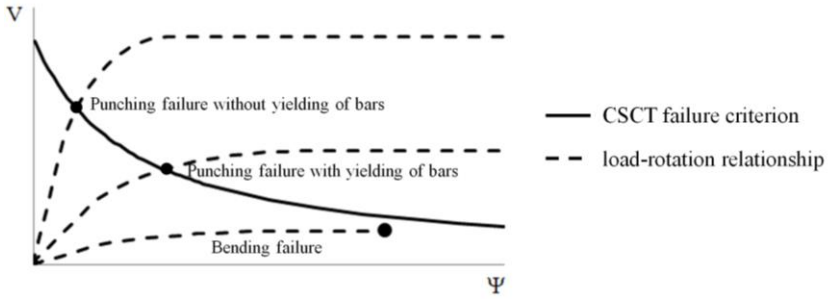

Figure 4 – CSCT failure criterion and different failure modes.

Figure 4 shows that the failure criterion can be intersected by the load-rotation curve before or after yielding of the flexural reinforcement. Eq.(2) tends to zero shear strength for large values of the rotation; however the slab is governed by bending when bar rupture or crushing of concrete, due to acting moment, occurs prior to reaching the failure criterion.

For design purposes, a characteristic failure criterion can be adopted [44], Eq.(3):

$$\frac{V_{Rd}}{b_0 \cdot d_v \cdot \dfrac{\sqrt{f_{ck}}}{\gamma_c}} = \frac{1}{1.5 + 0.9 \cdot \psi \cdot d \cdot k_{dg}} \tag{3}$$

being k_{dg} =36[mm]/(16+d_g), f_{ck} the characteristic value of the cylinder compressive strength of concrete, γ_c, the adopted value of the partial safety factor for concrete material properties (assumed equalto 1 and 1.5 for the evaluation of the characteristic and design punching shear resistance, respectively).

A modified failure criterion has been proposed by Maya et al. [45] for fibre-reinforced concrete slabs. In that case the punching shear resistance can be calculated as the sum of plain concrete and fibre contributions as given in Eq.(4):

$$V_R = V_{R,c} + V_{R,f} \tag{4}$$

where $V_{R,c}$ and $V_{R,f}$ are the contributions of plain concrete and fibres, respectively, see Figure 5.

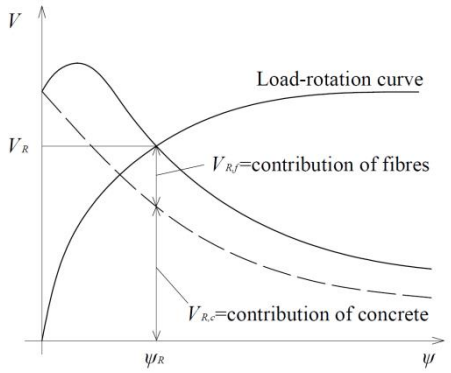

Figure 5 – Addition of concrete - and fibres contribution to the punching shear resistance.

In this paper the influence of the in-plane forces resulting from the CMA effect is considered in the derivation of the moment-rotation curve to be intersected with the CSCT failure criterion. In references [46] - [48] a modified failure criterion is proposed when axial forces are involved (for example in case of prestressed RC slabs). On the contrary in this paper it was assumed that the effect of CMA is only modifying the load deflection curve and does not influence the CSCT failure criterion. Neglecting the modification of the failure criterion due to axial forces leads to more conservative estimates of the punching shear resistance. Anyway this approach should be preferred in case of axial forces generate by CMA which may vary during the loading history due to their dependency on the slab deflection and second order effects.

3 Case studies modeling

In this paper, the multi-layered shell modeling, which adopts the PARC_CL crack model and post-processing of NLFEA results according to the CSCT theory, has been applied for the evaluation of bending and punching shear resistance of confined and unconfined circular slabs characterized by low CMA effects and tested at the Stevin Laboratory of Delft University of [12]. This first case study serves to demonstrate that the proposed procedure is in general able to predict both bending and punching failure load.

Subsequently the same procedure has been applied for the prediction of the non-linear behavior of the Corick bridge [1], to demonstrate the potential of the presented procedure to include CMA for a practical case.

3.1 Confined and unconfined circular specimens

The experimental program, reported in [12] consisted in total of 24 reinforced and fibre-reinforced concrete slabs; in this paper only the 18 specimens cast with normal aggregate concrete are considered.

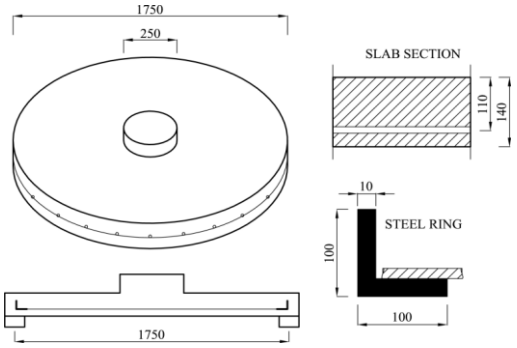

Figure 6 - Experimental set-up for circular slabs [12].

The slab diameter was 1750 mm and the total cross-sectional depth was 140 mm (Figure 6). The specimens were simply supported along their edges and were subjected to a concentrated load in the center, applied through a cylindrical stub with a diameter of 250 mm and a depth of 200 mm. The details of all specimens are summarized in Table 1 and in Table 2. The slabs were all reinforced with orthogonal nets; in Table 1 the yield strain, ε_y, the strain at maximum force, ε_u, the yield strength, f_y, the bar diameter, ϕ, the bar distance, p, and the reinforcement ratio, ρ, are reported. The fibres used had a length, L_f, equal to 50 mm and a diameter, d_f, equal to 0.8 mm; the fibre content is indicated in Table 1. In Table 1 and Table 2 the average cube compressive strength, $f_{c,cube}$, and splitting tensile strength, $f_{ct,sp}$, experimentally measured are listed together with the cylinder compressive strength, f_c, the Young's modulus, E_c, and the axial tensile strength f_{ct}, obtained from Model Code 2010 [42] formulations. For all the slabs maximum aggregate size was equal to 16 mm.

Specimens 1 to 9 were unconfined: this series of specimens was subdivided into three subseries of specimens having different reinforcement ratios (0.089%, 0.998% and 1.837%); each subseries consisted of three specimens with different fibre contents (0, 40 and 80 kg/m^3). Specimens 11 to 19 were confined by a restraining steel ring connected to the reinforcement by welding: this series of specimens was subdivided into three subseries having the same reinforcement ratios and fibre contents as the unconfined specimens.

Table 1 - Details of unconfined specimens.

Spec.	Concrete					Steel						Fibre content
	$f_{c,cube}$ [Mpa]	f_c [Mpa]	E_c [Mpa]	$f_{ct,sp}$ [Mpa]	f_{ct} [Mpa]	ε_y [-]	ε_u [-]	f_y [Mpa]	ϕ [mm]	p [mm]	ρ [%]	[kg/m^3]
1	36.28	30.11	31047	2.74	2.466	0.0030	0.0075	600	5	200	0.089	0
2	49.23	40.86	34372	3.71	3.339	0.0030	0.0075	600	5	200	0.089	40
3	46.9	38.93	33821	3.39	3.051	0.0030	0.0075	600	5	200	0.089	80
4	41.38	34.35	32439	2.86	2.574	0.0024	0.0275	480	12	103	0.998	0

5	46.95	38.97	33833	3.13	2.817	0.0024	0.0275	480	12	103	0.998	40
6	48.49	40.25	34199	3.47	3.123	0.0024	0.0275	480	12	103	0.998	80
7	47.45	39.38	33953	2.91	2.619	0.0024	0.0275	480	16	99.56	1.837	0
8	45.12	37.45	33388	3.28	2.952	0.0024	0.0275	480	16	99.56	1.837	40
9	45.12	37.45	33388	3.26	2.934	0.0024	0.0275	480	16	99.56	1.837	80

Table 2 - Details of confined specimens.

Spec.	Concrete					Steel						Fibre content
	$f_{c,cube}$ [Mpa]	f_c [Mpa]	E_c [Mpa]	$f_{ct,sp}$ [Mpa]	f_{ct} [Mpa]	ε_y [-]	ε_u [-]	f_y [Mpa]	ϕ [mm]	p [mm]	ρ [%]	[kg/m^3]
11	39.1	32.45	31831	2.44	2.196	0.0030	0.0075	600	5	200	0.089	0
12	49.23	40.86	34372	3.41	3.069	0.0030	0.0075	600	5	200	0.089	40
13	48.53	40.28	34209	3.65	3.285	0.0030	0.0075	600	5	200	0.089	80
14	41.38	34.35	32439	2.86	2.574	0.0024	0.0275	480	12	103	0.998	0
15	46.96	38.98	33836	3.13	2.817	0.0024	0.0275	480	12	103	0.998	40
16	49.66	41.22	34472	3.47	3.123	0.0024	0.0275	480	12	103	0.998	80
17	45.03	37.37	33366	3.1	2.79	0.0024	0.0275	480	16	99.56	1.837	0
18	45.4	37.68	33457	3.61	3.249	0.0024	0.0275	480	16	99.56	1.837	40
19	48.22	40.02	34136	3.41	3.069	0.0024	0.0275	480	16	99.56	1.837	80

For the analyses all specimens were modeled with three-node multi-layered shell elements (S3), Figure 7(a). Over its thickness each shell element was divided into three layers: the first and the third layers consisted of plain concrete, while the second layer was a reinforced concrete layer; the reinforcement was smeared according to the PARC_CL model hypothesis. Five Simpson integration points were used over the thickness of each layer, Figure 7(b). The slabs were considered simply supported along their edge: that means that fixed boundary conditions which prevented displacements along the vertical axis, *3*, apply to nodes placed at a distance of 830 mm from the center of the slab. For the confined slabs, the steel ring was modeled with beam elements having an equivalent area equal to 1900 mm^2 and a modulus of elasticity equal to 200000 MPa.

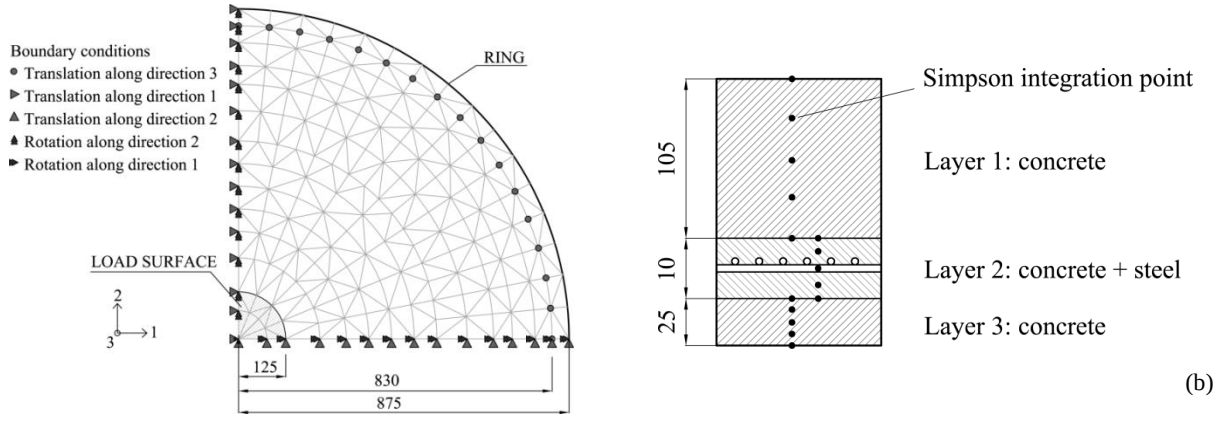

Figure 7 - (a) Slab modeling and (b) Position of integration points along the thickness in multi-layered shell elements.

In the first step of the NLFE analyses the self-weight of the slabs (equal to 8,41 KN) was applied: in the second step a pressure was applied to the area experimentally loaded through the stub. A standard Newton-Raphson convergence criterion was adopted for the incremental iterative process.

In Figure 8 the comparisons between experimental and NLFEA load-deflection curves are reported for confined and unconfined specimens. In general, it can be noted that for specimens characterized by low reinforcement percentages and bending failures NLFE analyses well predicts the peak load values, whereas on the contrary, for the specimens characterized by high reinforcement percentages and punching failures the slab resistance cannot be properly determined with shell modeling and it is necessary to adopt a post processing procedure using the CSCT failure criterion.

Figure 8 shows that the stiffness of the steel ring that was used in the experimental tests to restraint the radial displacements is small when compared with the stiffness of confining elements found in bridge deck slabs or real flat slabs in buildings. It is clear from the test results that the confinement provided by the steel ring is only significant for the lightly reinforced slabs (ρ = 0.089%), which actually seem to fail in bending. However the main goal of this section was to demonstrate that NLFEA results, properly post-processed according to CSCT, can be used for the punching shear resistance assessment. In the next section the confinement effect in case of continuous slabs will be analysed.

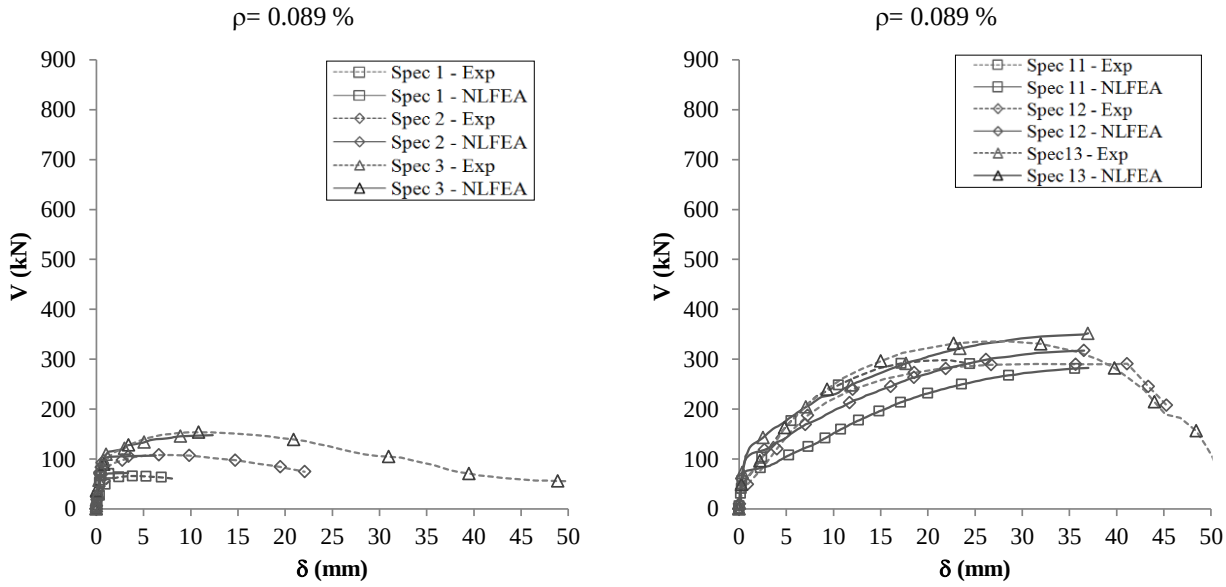

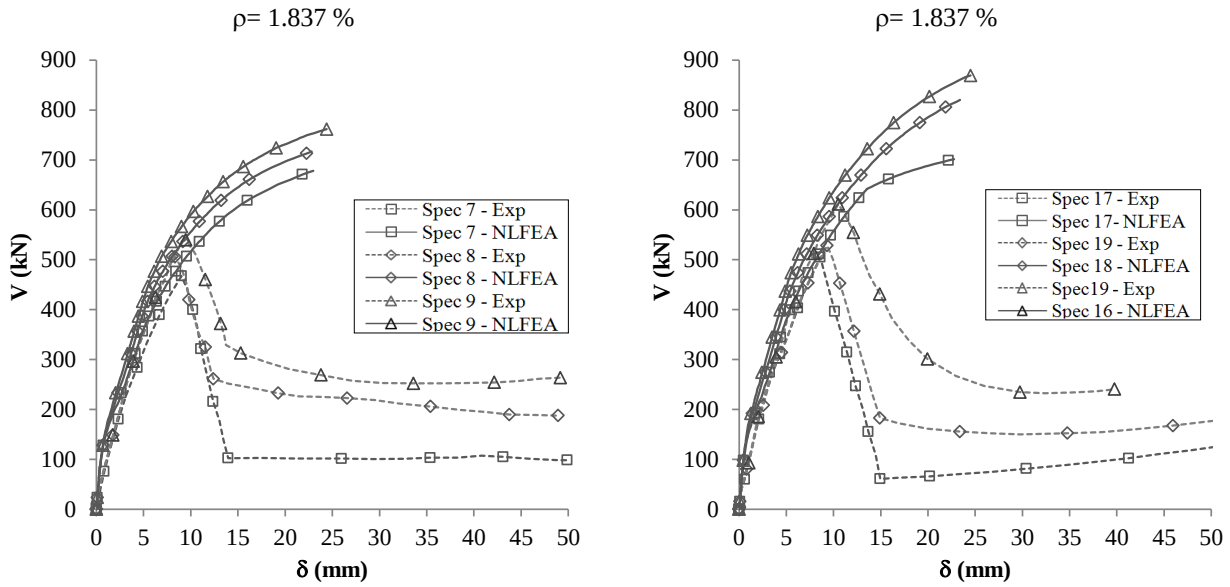

Figure 8 - Comparison between experimental and calculated load-deflection curves for a) unconfined and b) confined specimens.

In Figure 9 the load-rotation curves obtained using the analytical procedure proposed in [39] are plotted together with the load-rotation curves obtained from NLFEA results. The rotation of the slabs obtained from NLFEA results was measured in correspondence of the slab perimeter.

Figure 9 illustrates that the V-ψ curves obtained with NLFEA are in good agreement with the V-ψ curves obtained with the analytical approach proposed in [39] for specimens without ring; their intersection with the failure criterion occurs for approximately similar loads, providing about similar punching shear resistances.

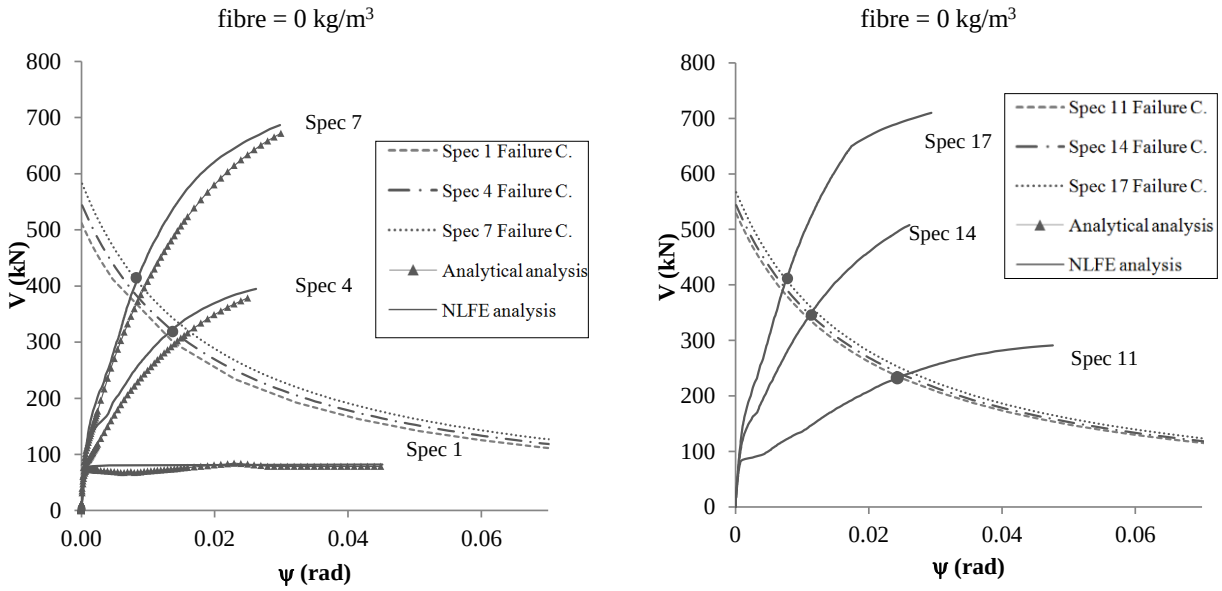

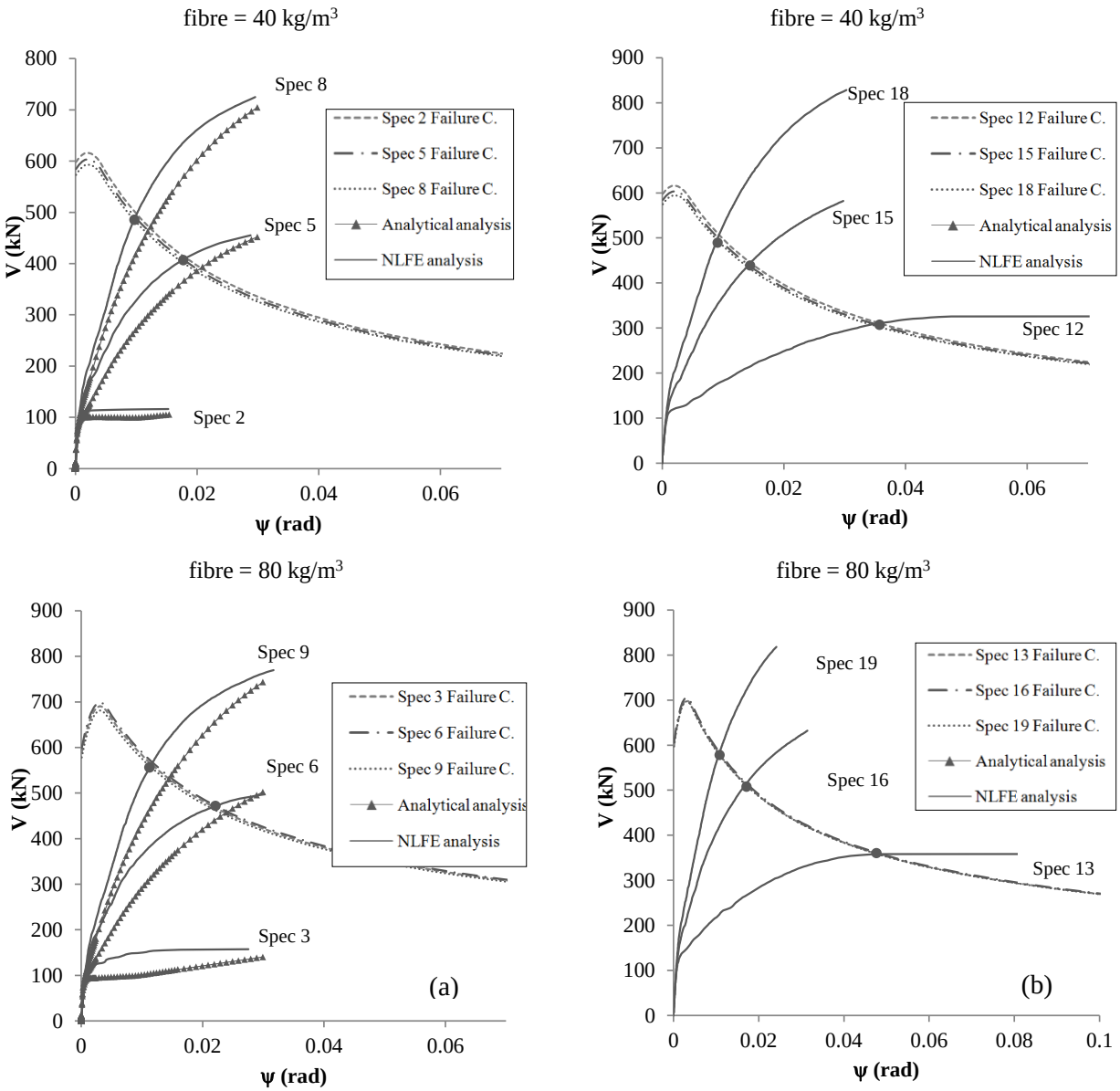

Figure 9 - Load - rotation curves for specimens a) without ring and b) with ring.

In Table 3 the ultimate load measured from the tests, V_{test}, calculated according to [39] using analytical calculations, V_{CSCT}, and obtained from NLFEA using multi-layered shell elements and PARC_CL crack model, $V_{NLFEA/CSCT}$, are summarized for specimens without ring.

Comparisons between the experimental ultimate load and the numerical values achieved using analytical and NLFEA results show that both models are well predicting the measured strengths and are on the safe side.

Table 3 - Comparison between experimental, numerical and analytical results for specimens without ring.

Spec.	V_{test} [kN]	$V_{NLFEA/CSCT}$ [kN]	$V_{test}/V_{NLFEA/CSCT}$ [-]	V_{CSCT} [kN]	V_{test}/V_{CSCT} [-]	Failure
1	65.5	61.58	/	/	/	B
2	109.7	97.58	/	/	/	B
3	157.1	148.00	/	/	/	B
4	405.5	321.41	1.26	307.96	1.32	P

5	461.8	407.61	1.13	387.88	1.19	P
6	453.3	471.55	0.96	458.76	0.99	B/P
7	467.2	409.43	1.14	394.92	1.18	P
8	502.8	485.31	1.04	459.24	1.09	P
9	540.4	558.5	0.97	527.12	1.03	P
		Average	1.08	Average	1.13	
		COV	0.098	COV	0.098	

In Table 3 the average ratio of effectiveness and the coefficient of variation, COV, are presented for slabs characterized by punching shear failure mode. NLFEA results are closer to the test strengths than analytical calculation; indeed Table 3, shows that the average value of $V_{test}/V_{NLFEA/CSCT}$ is closer to 1.0 than the average value of V_{test}/V_{CSCT}. Furthermore the Coefficient of Variation of $V_{test}/V_{NLFEA/CSCT}$ values results to be in this case equal to the Coefficient of Variation of V_{test}/V_{CSCT} values.

Table 4 - Comparison between experimental and numerical results for specimens with ring.

Spec.	V_{test} [kN]	$V_{NLFEA/CSCT}$ [kN]	$V_{test}/V_{NLFEA/CSCT}$ [-]	Failure
11	291.4	234	1.25	B/P
12	299.6	310.82	0.96	B/P
13	335.4	358.01	0.94	B/P
14	459.9	346.6	1.33	P
15	469.6	439.84	1.07	P
16	550.2	514.94	1.07	P
17	505	409.36	1.23	P
18	530.9	495.49	1.07	P
19	612.2	579.73	1.06	P
		Average	1.11	
		COV	0.11	

In Table 4 the ultimate load measured from the tests, V_{test}, and obtained from NLFEA using multi-layered shell elements and PARC_CL crack model, $V_{NLFEA/CSCT}$, are summarized for specimens with ring. The analytical calculations, V_{CSCT}, were not carried out because the evaluation of the effects of varying compressive stresses should be properly considered. These latter calculations are out of the scope of this paper, the reader can refer to [46] and [47] for analytical calculations.

NLFEA results are close to test measurements also in case of specimens with ring; indeed Table 4 shows that the average value of $V_{test}/V_{NLFEA/CSCT}$ equals 1.1 and the Coefficient of Variation of $V_{test}/V_{NLFEA/CSCT}$ values equals 0.11.

3.2 Evaluation of proof loading tests on an existing bridge deck

In [1] in situ proof loading of Corick Bridge in Northern Ireland is reported. Proof loading was carried out in order to demonstrate that the bridge deck is able to resist at least three times the design wheel load as prescribed in the UK Code. It was supposed that CMA would play a substantial role in

the bearing capacity of the bridge deck. Corick bridge consists of five I-shaped prestressed concrete beams supporting a 160 mm in-situ reinforced concrete deck slab. The bridge deck was subdivided into 12 slabs having different reinforcement ratios, reinforcement layouts, concrete compressive strengths and polypropylene fibre volume, Figure 10. The geometrical and mechanical properties are summarized in Table 5.

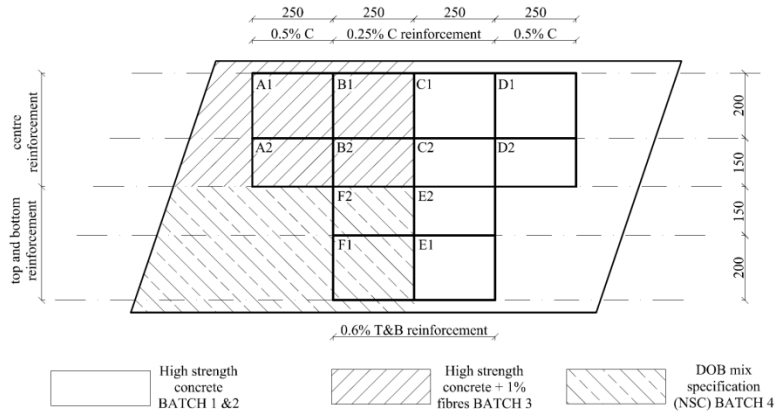

Figure 10 - Test panel arrangement (dimensions in cm).

Each slab was loaded as depicted in Figure 11; the loading sequence consisted of two steps: slabs were loaded to a level just beyond the cracking load (initial cracking load tests) and subsequently the load was removed and the slabs were re-loaded again to a higher level (full test load); deflections and strains were recorded after each load increment.

The British code BD81/02 prescribes a maximum wheel design load equal to 112.5 kN for design, but each slab was loaded to at least 333 kN (Table 4), which is three times the maximum wheel load (in order to demonstrate that a safety margin of at least a factor 3.0 is obtained). At the end of the tests none of the slabs presented substantial signs of upcoming failure, demonstrating the existence of the target safety margin at least 3.0.

Table 5 - Geometrical and mechanical properties.

Test panel	Concrete batch no.	Compressive strength of concrete, f_c [N/mm^2]	Deck slabs reinforcement	Effective depth, d [mm]	Slab clear span [mm]	Max exp load value [kN]
A1	3	56.2	0.5% C +fibers	82	1740	333
A2	3	58.2	0.5% C +fibers	74	1240	428
B1	3	55.3	0.25% C +fibers	75	1740	344
B2	3	59.5	0.25% C +fibers	75	1240	428
C1	1	58.7	0.25% C	75	1740	333
C2	1	56.5	0.25% C	75	1240	428
D1	1	53.9	0.50% C	75	1740	368
D2	1	53.9	0.50% C	75	1240	428
E1	2	49	0.60% T&B	105	1740	392

E2	2	49	0.60% T&B	105	1240	428
F1	4	41.9	0.60% T&B	103	1740	371
F2	4	44.1	0.60% T&B	103	1240	428

(C = single layer of reinforcement at mid depth, Figure 13(a); T&B = top and bottom layers of reinforcement, Figure 13(b))

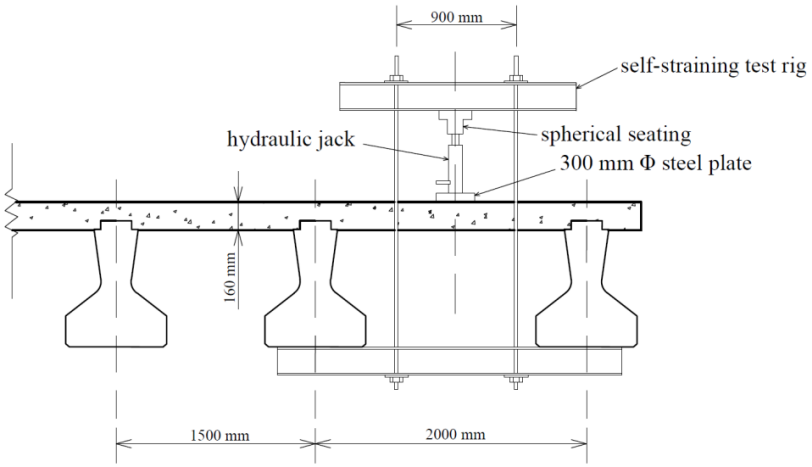

Figure 11 - Bridge deck cross section and typical test arrangement.

The entire bridge was modelled with 4-nodes and 3-nodes linear shell elements. The girders were modeled with rectangular 4 nodes elements with different thicknesses according to the girders geometry. The girders were considered simply supported at their ends. The modelling of the experimental setup, shown in Figure 11, was simplified by applying a fixed boundary condition, to one node of each girder, which restrained the vertical displacement of girders supporting the loaded slabs. These boundary conditions were applied only to the two nodes aligned with the point of application of the load. A finer mesh of non-linear multi-layered shell elements was adopted only for a limited part of the bridge corresponding to the loaded slab. Figure 12 shows the mesh adopted for the entire bridge and the loaded slab F2 (see also Figure 10).

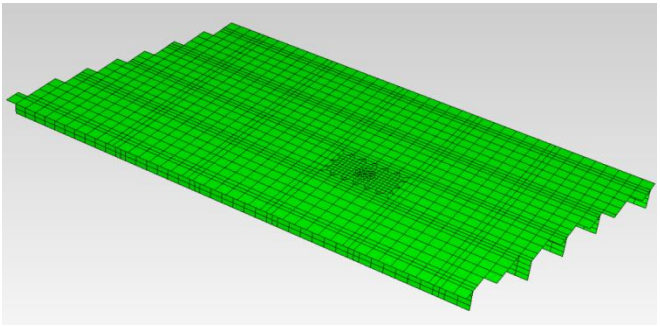

Figure 12 - Mesh adopted for the entire bridge with loaded panel F2.

Over its thickness each shell element was subdivided into two or three layers depending respectively on the type of reinforcement, being either a single layer in the centre of the slab 'C', or a double layer in the top and bottom of the slab 'T & B', as denoted in Table 4 (see Figure 13).

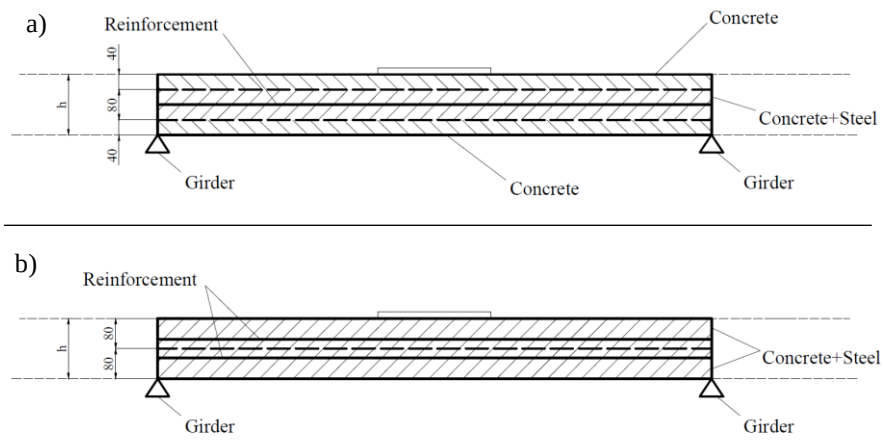

Figure 13 - Layer configuration for a) single layer of reinforcement panel (denoted as "C" in Table 5), b) double layer reinforcement (denoted as "T&B" in Table 5).

A reduced Gaussian integration scheme in the element plane, and a Simpson integration scheme with five integration points for each layer was adopted over the thickness.

Comparisons between experimental and NLFEA calculated load-vertical deflection curves are shown for two panels (C1 & F2), in Figure 14. The good fitting between experimental and NLFEA results demonstrates that the proposed multi-layered shell modeling with the PARC_CL crack model is able to predict the non-linear behavior of RC slabs with good accuracy.

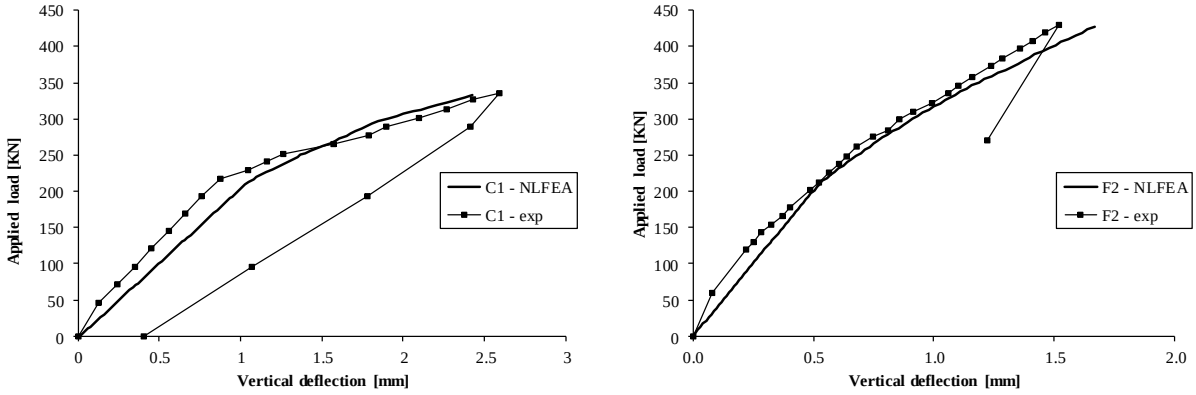

Figure 14 – Comparison between experimental and NLFEA results for the Corick bridge [1].

In order to consider the effect of Compressive Membrane Action on the slab behavior, three different models were used. The model called '*Entire bridge'* was the model representing the whole bridge; the model called '*Fixed strip*' was obtained by meshing only a strip of the slab by applying fixed boundary conditions which restrained all the displacements and rotations at the supports; the model called '*Roller strip*' was equal to the model '*Fixed slab*', but with released horizontal displacements at supports (nodes were free to move along the horizontal axes), Figure 15.

The response of the 'Entire bridge' model was examined as the control level against which the other models were compared.

The response of the '*Fixed strip*' model was examined to investigate the influence of girders and adjacent panels on the slab behavior; while the response of the '*Roller strip*' was investigated to recognize the influence of only lateral confinement on the slab resistance.

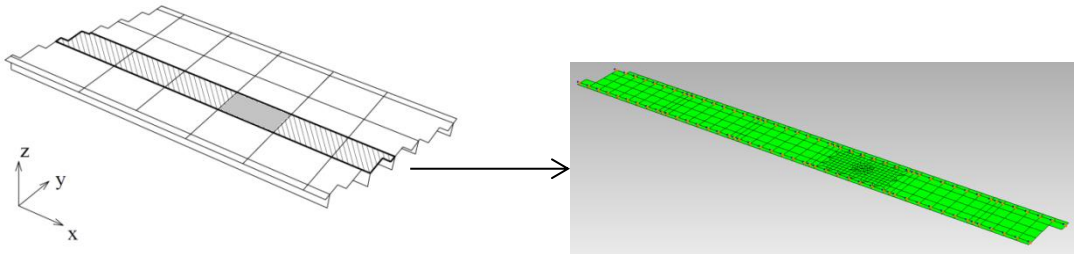

Figure 15 – Example of strip.

In order to achieve the punching shear resistance value, Figure 16 shows the intersections between the CSCT failure criterion and the NLFEA load-rotation curves obtained with the different models for the Corick bridge. The rotation of the slabs was obtained from the values of NLFEA rotations at nodes placed in correspondence of the position where the radial bending moment is zero. The failure criterion is evaluated by assuming the effective depth value, d, given in Table 5 and the shear-resisting effective depth, d_v, equal to 0.9 the slab depth. The shear resisting control perimeter, b_0, was calculated at a distance 0.5 d_v from the loading steel plate and results to be a constant value for all the analysed slabs.

It can be seen that the punching shear resistance values, obtained using the *"Entire bridge"* and *"Fixed strip"* models do not differ much. However, the punching shear resistance obtained using the 'Roller strip' model was generally significantly lower.

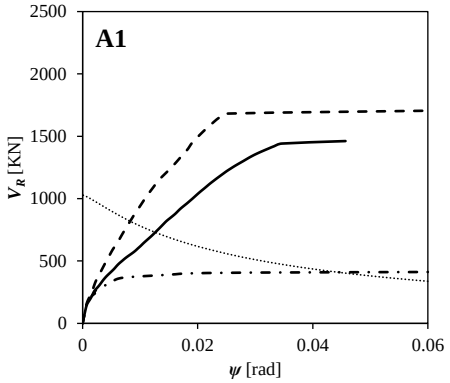

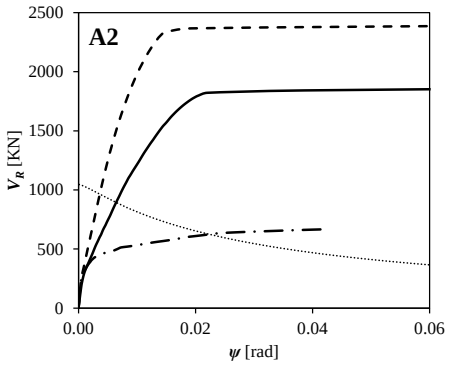

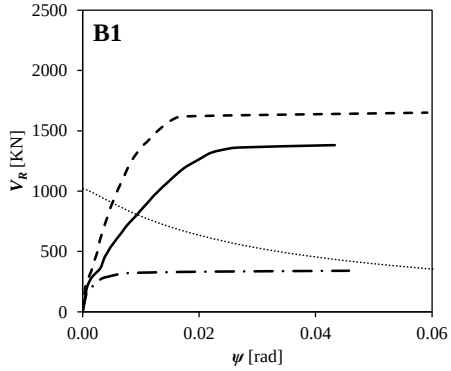
B1
2500
2000
1500
1000
500
0
V_R [KN]
0.00
0.02
0.04
0.06
ψ [rad]

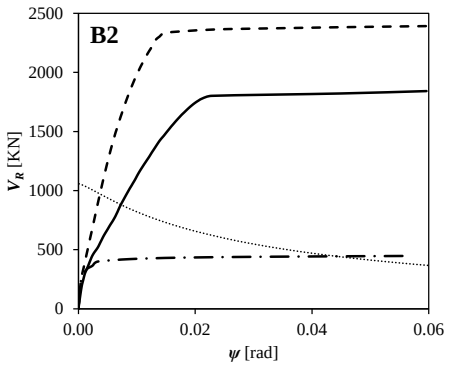
B2
2500
2000
1500
1000
500
0
V_R [KN]
0.00
0.02
0.04
0.06
ψ [rad]

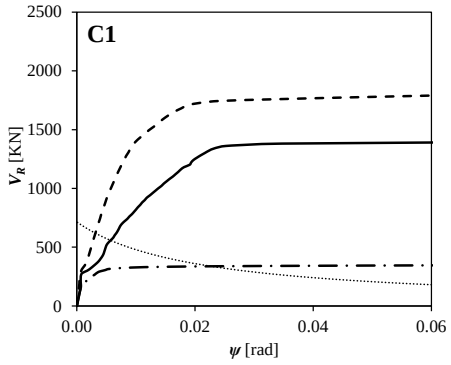
C1
2500
2000
1500
1000
500
0
V_R [KN]
0.00
0.02
0.04
0.06
ψ [rad]

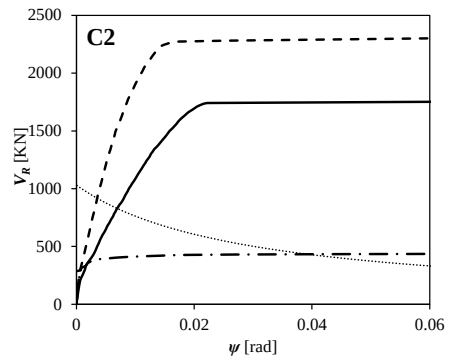
C2
2500
2000
1500
1000
500
0
V_R [KN]
0
0.02
0.04
0.06
ψ [rad]

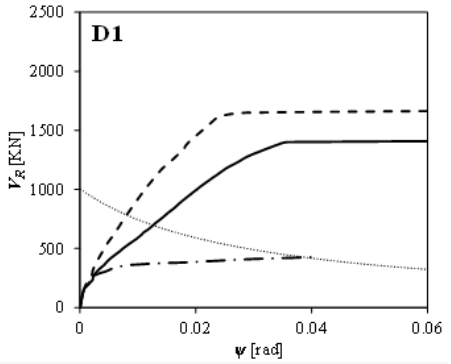
D1
2500
2000
1500
1000
500
0
V_R [KN]
0
0.02
0.04
0.06
ψ [rad]

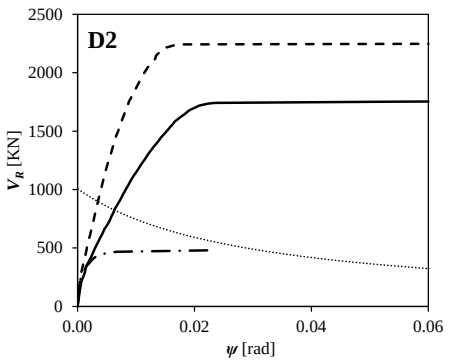
D2
2500
2000
1500
1000
500
0
V_R [KN]
0.00
0.02
0.04
0.06
ψ [rad]

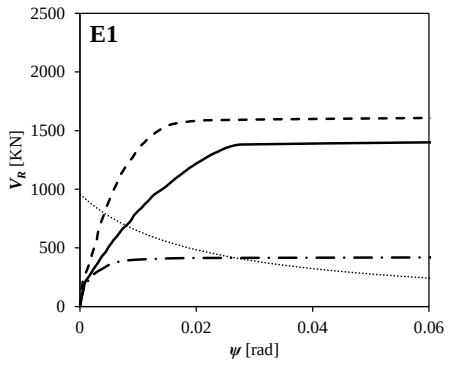
E1
2500
2000
1500
1000
500
0
V_R [KN]
0
0.02
0.04
0.06
ψ [rad]

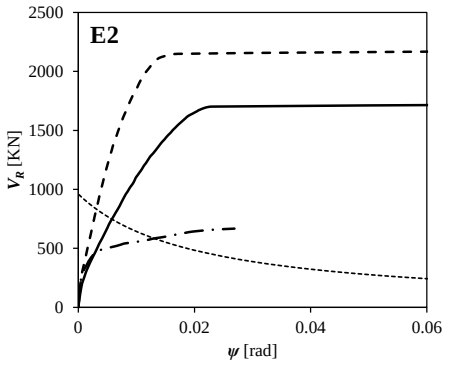
E2
2500
2000
1500
1000
500
0
V_R [KN]
0
0.02
0.04
0.06
ψ [rad]

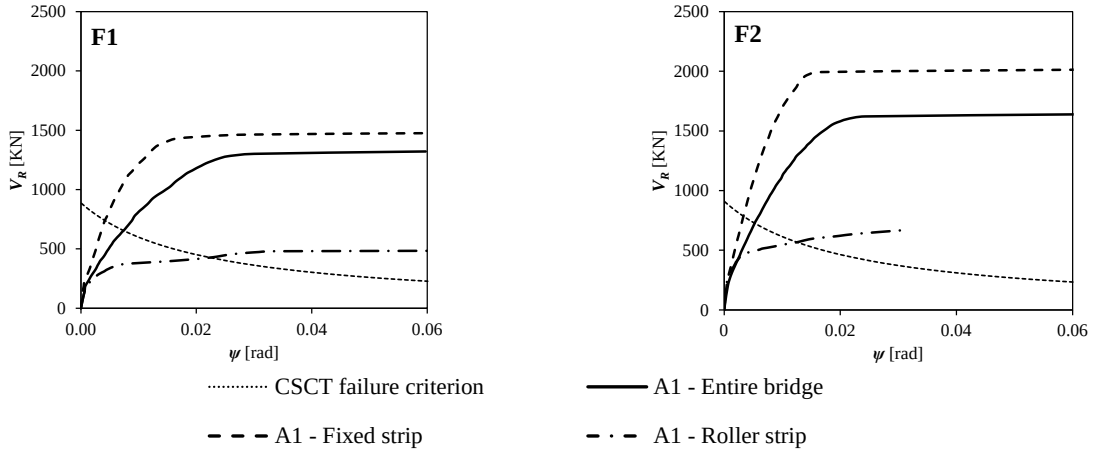

Figure 16 – Corick bridge response prediction obtained with different NLFE modelling.

3.2.1 Comparison between design punching shear resistances obtained with NLFE analyses and BD81/02 prescriptions

The design punching shear resistance was herein calculated according to British Code BD81/02 formulations and using NLFEA results properly handled according to safety formats.

Indeed, the design punching shear resistance can be calculated, in case of verifications assisted by NLFE analyses, by probabilistic analysis following safety format methods, as indicated by Model Code 2010 [42]. Furthermore, in the framework of Model Code 2010, LoA IV can be used to calculate the rotation of the slab with NLFE analyses.

Comparison between the design resistances obtained using BD81/02 code and NLFEA results were provided in this paper to check if design verifications can be safety carried out with the slab strengths achieved using LoA IV.

3.2.1.1 BD81/02 prescriptions

BD81/02 is the only European Code that recognizes the benefits of Compressive Membrane Action [2] on the base of the work done in [28] and [20]. The punching shear resistance for a circular load or a single wheel load is given by Eq.(5):

$$V_{Rd,BD81/02} = 1.52 \cdot (\varphi + d) \cdot d \cdot \sqrt{f_{cd}} \cdot (100 \cdot \rho_e)^{0.25} \tag{5}$$

where φ is the diameter of the loaded area, d is the average effective depth to the tensile reinforcement of the slab, f_{cd} is the design compressive strength of the concrete ($f_{cd} = f_{ck} / \gamma_m$), and ρ_e is the effective reinforcement ratio given by Eq.(6):

$$\rho_e = k \cdot \left[\frac{f_{cd}}{240} \right] \cdot \left[\frac{h}{d} \right]^2 \tag{6}$$

The non-dimensional arching moment coefficient, *k*, was obtained starting from the relationship between plastic strain ε_c and compressive strength of concrete, as given in Eq.(7), [28]:

$$\varepsilon_c = \left(-400 + 60 \cdot f_{cd} - 0.33 \cdot f_{cd}^2\right) \cdot 10^{-6} \tag{7}$$

This expression is valid for an idealized elastic-plastic concrete stress block for compressive strengths of concrete up to 70 N/mm^2. Eq.(8) allows calculating the non-dimensional parameter for the arching moment of resistance, *R*, Eq.(6), which is included in Eq.(9) for the evaluation of the parameter *k*:

$$\mathrm{R} = \frac{\varepsilon_c \cdot \mathrm{L}_r^2}{\mathrm{h}^2} \tag{8}$$

$$k = 0.0525 \cdot \left(4.3 - 16.1\sqrt{3.3 \cdot 10^{-4} + 0.1243 \cdot R}\right) \tag{9}$$

being L_r the half of the span.

BD81/02 establishes some limitations on the use of its proposed theory, [2]. For example the dimension of the slab panel perpendicular to the direction of traffic should not exceed 3.7 m; the slab shall extend at least 1m beyond the center line of the external longitudinal supports of a panel in order to provide sufficient confinement; the span length to thickness ratio of the slab should not exceed 15; the minimum reinforcement ratio should be at least 0.3%. It should be also remarked that BD81/02 formulation doesn't include size effect.

3.2.1.2 Safety formats: ECOV method

In *fib*-Model Code 2010 several safety formats are presented, in this paper the Method of Estimation of Coefficient of Variation of resistance (ECOV) was adopted to evaluate the design shear punching resistance of the Corick bridge. This procedure was checked for isolated slabs in by comparing the design punching shear resistance obtained with different safety formats [49].

To this aim the estimates of the mean and characteristic values of resistance have been obtained by using the corresponding values of material parameters, Eq.(10), [42]:

$$V_{Rm} = r\left(f_m, \ldots\right), \quad V_{Rk} = r\left(f_k, \ldots\right) \tag{10}$$

The resistance of the slab was obtained by intersecting the CSCT failure criterion with the load versus rotation relation of the slab obtained from NLFEA results.

Both NLFEA load versus rotation relation and CSCT failure criterion were derived from mean and characteristic strength values to achieve, respectively, the mean and characteristic values of resistance R_m and R_k. The failure criterion adopted taking account of average and characteristic material properties is obtained from Eq.(2) and Eq.(3) , respectively. The coefficient of variation of resistance, v_R, is given by Eq.(11):

$$v_R = \frac{1}{1.65} ln\left(\frac{V_{Rm}}{V_{Rk}}\right) \tag{11}$$

The global resistance factor γ_R for the mean value is determined from Eq.(12):

$$\gamma_R = exp(\alpha_R \cdot \beta \cdot v_R) \tag{12}$$

being α_R=0.8 and β=3.8. Finally the design punching shear resistance of the slab is calculated from Eq.(13):

$$V_{Rd,LevelIV} = \frac{V_{Rm}}{\gamma_{Rd} \cdot \gamma_R} \tag{13}$$

being γ_{Rd} equal to 1.06.

Table 6 summarizes punching shear resistances obtained with BD81/02 and LoA IV which refers to NLFEA results of the *'Entire bridge'* model.

Table 6 – Comparison between design punching shear resistances obtained with BD81/02 and LoA IV.

	$V_{Rd,BD81/02}$ [kN]	V_{Rm} [kN]	V_{Rk} [kN]	$V_{Rd,Level\ IV}$ [kN]	$V_{Rd,Level\ IV}/V_{Rd,BD81/02}$ [-]
A1	363.99	729	583	456	1.25
A2	366.27	894	720	566	1.55
B1	350.10	805	641	499	1.43
B2	390.47	881	719	572	1.46
C1	366.39	788	620	478	1.30
C2	374.28	829	647	495	1.32
D1	343.23	697	490	344	1.00
D2	359.95	824	649	501	1.39
E1	392.25	690	499	358	0.91
E2	409.18	747	601	472	1.15
F1	339.83	654	501	378	1.11
F2	368.02	726	559	423	1.15
				Average	1.25

It can be observed that, as expected, the design punching shear resistance values obtained by numerical simulation are higher than the design values obtained with the analytical calculations; the mean value of the ratio $V_{Rd,Level\ IV}/V_{Rd,BD81/02}$ is equal to 1.25. The appropriateness of the design values according to BD81/02 was confirmed by the maximum loads reached during proof loading. The design values obtained with the numerical method have been obtained taking account of the real dimensions and boundary conditions of the bridge deck, whereas the results according to BD81/02 are obtained assuming more general boundary conditions, which explains the larger safety margin, as confirmed by Table 6, last column.

In Table 7 the design punching shear resistances obtained using the LoA IV which refer to NLFEA results of the *'Entire bridge'* model, the *'Fixed strip'* model and '*Roller strip*' model, are reported. The design punching shear resistance is normalized to the design punching shear resistances calculated from NLFEA results of the *'Entire bridge'* model.

The design punching shear resistance obtained with '*Roller strip*' model is too conservative because it is unable to properly include CMA effects.

The *"Fixed strip"* model provides design punching shear resistance values close to the values obtained with the *'Entire bridge'* model, meaning that this simplified model, which requires lower computational efforts, could safely be accepted for the determination of the design resistance.

Table 7 – Comparison between design punching shear resistances evaluated using the LoA IV and different modelling of the bridge deck slab.

	'Entire bridge' model	*'Roller strip'* model		*'Fixed strip'* model	
	$V_{Rd,\ entire\ bridge}$ [kN]	$V_{Rd,\ roller\ strip}$ [kN]	$V_{Rd,roller\ strip}/V_{Rd,entire\ bridge}$ [-]	$V_{Rd,\ fixed\ strip}$ [kN]	$V_{Rd,fixed\ strip}/V_{Rd,entire\ bridge}$ [-]
A1	456	391	0.86	498	1.09
A2	566	422	0.75	605	1.07
B1	499	223	0.45	559	1.12
B2	572	300	0.52	613	1.07
C1	478	245	0.51	559	1.17
C2	495	277	0.56	555	1.12
D1	344	285	0.83	469	1.36
D2	501	438	0.87	549	1.10
E1	358	291	0.81	384	1.07
E2	472	392	0.83	495	1.05
F1	378	281	0.74	418	1.11
F2	423	379	0.89	451	1.07
		Average	0.72	Average	1.12

4 Conclusions

In this paper a multi-layered shell model, including the PARC_CL crack model, is proposed for the evaluation of the flexural and shear resistance of RC slabs according to CSCT theory. The effectiveness of the presented procedure, which also includes CMA effects, is verified by comparing NLFEA results with experimental observations on confined and unconfined circular slabs and bridge deck slabs. The main advantage inherent in the use of a multi-layered shell modelling of a real structure (like a bridge) is the ability to adopt the same model to predict both the global non-linear behavior and the local failure modes due to concentrated loads. Furthermore, the effect of compressive membrane action on structural resistance assessment can be properly taken into account with the proposed method, because compressive actions automatically arise from the boundary and

loading conditions of the model. The application of multi-layered shell modeling for the prediction of both punching and flexural resistance of RC slabs according to the CSCT theory offers several advantages. First of all, models able to predict the non-linear flexural behavior (without considering the shear failure) are required for the application of the CSCT approach. These latter models are usually more user-friendly than crack models implemented to analyze shear failure, whose results are rather dependent on material models and geometrical uncertainties. The verification assisted by numerical simulation, as stated in [10], should give results which are stable and less sensitive to material models and analyst choices done during the NLFE modeling process. Furthermore the non-linear behavior of multi-layered shell elements is described with crack models implemented for a plane state of stress (2D) which are usually more comprehensive than 3D crack models.

The comparison between NLFEA results, experimental observations and analytical results obtained using the British Code BD81/02 formulations demonstrate that the proposed multi-layered shell modelling combined with the CSCT failure criterion can be an useful tool for the evaluation of the flexural and/or shear capacity of RC slabs subjected to concentrated loads and characterized by arbitrary boundary conditions. It can be noted that the results of punching shear resistance using LoA IV are higher than those obtained using BD81/02 (Table 5) because the process behind NLFEA takes account of more parameters than considered in the BD81/02 calculation. The equality of punching shear resistance results given from the *'Entire bridge'* model and the *'Fixed strip'* model (Table 6) indicates that modelling only the fixed supported bridge deck strip could be a suitable way of predicting the local failures occurring in the deck, due to concentrated loads; however, the same aim can be achieved by modelling the entire bridge, in addition to the prediction of the global behavior of the structure. In any case, the conclusion that the fixed strip model can be used to estimate the shear safety may not be generalizable to other bridge configurations and depends on the amount of restraint. In general, this gives certainly an upper bound to the real failure load and not always a "safe" estimate.

The *'Roller strip'* results were the most conservative because their boundary conditions did not take account for CMA. The relatively high values of $V_{Rd,Level\ IV}/V_{Rd,BD81/02}$ ratio for fibre-reinforced concrete slabs (Table 6 - A1, A2, B1, B2) are probably due to the fact that the BD81/02 method does not take account of the effect of fibres inside concrete.

The results obtained with BD81/02 and the multi-layered shell and PARC_CL crack model combined with the CSCT failure criterion are very near to each other although these methods have been derived on a totally different basis. This indicates that both methods are reliable, however, the multi-layered shell and PARC_CL crack model combined with the CSCT failure friterion has a broader validity, and can be used for any slab geometry and loading condition, as it is applicable outside the calibrated region of the BD81/02 analytical formulation.

5 References

[1] Taylor S.E., Rankin B., Cleland D.J., Kirkpatrick J. Serviceability of Bridge Deck Slabs with Arching Action. ACI Struct J 2007; 104(1): 39-48.
[2] U.K. Agency. BD 81/02: Use of Compressive Membrane Action in Bridge Decks. Design Manual for Roads and Bridges 2002; 3: 11.1-11.5.
[3] Rankin G.I.B. and Long A.E. Predicting the enhanced punching strength of interior slab-column connections, Proceedings of the Institution of Civil Engineers, 1987;Vol 82(1): 1165-1186.
[4] Bailey C.G. Membrane action of unrestrained lightly reinforced concrete slabs at large displacements. Eng Struct 2001; 23: 470-483.
[5] Dat P.X., Hai T.K.. Membrane action of RC slabs in mitigating progressive collapse of building structures. Eng Struct 2013; 55: 107-115.
[6] Eyre J. Membrane action in isotropic patch-loaded unrestrained slabs. Magazine of Concrete Research 2006; 58(6): 357-366.
[7] C.S. Association. Canadian Highway Bridge Design Code (CHBDC), CAN/CSACSAS6-00 (R2005), Canada.
[8] T.N.Z.A. Aotearoa. New Zealand Bridge Manual, 2nd edition. 2003.
[9] Gvodzev A. The Determination of the value of the collapse load for statically indeterminate systems undergoing plastic deformation. International Journal of Mechanical Sciences 1936; 1: 322-335.
[10] Braestrup, M.W. Dome Effect in RC Slabs: Rigid-Plastic. ASCE J Struct Div 1980; 106(ST6): 1237-1253.
[11] Vecchio F., Collins M. Investigating the collapse of a warehouse. Concrete International 1990; 12(3): 72-78.
[12] Walraven J.C., Pat T., Markov I. The punching shear resistance of fibre reinforced concrete slabs. in RILEM Symposium - Developments in fibre reinforced cement and concrete, 1986, Sheffield.
[13] Rankin G.I.B., Niblock R.A., Skates A.S. and Long A.E. Compressive Membrane Action Strength Enhancement in Uniformly Loaded, Laterally Restrained Slabs. The Struct Eng 1991; 69(16/20):287-295.
[14] Salim W., Sebastian W. Punching Shear Failure in Reinforced Concrete Slabs with Compressive Membrane Action. ACI Struct J 2003; 100(4): 471-479.
[15] Fang I.K., Lee J.H., Chen C.R. Behavior of Partially Restrained Slabs under Concentrated Load. ACI Struct J 1994; 91(2): 133-139.
[16] Taylor S., Rankin G., Cleland D. Arching action in high-strength concrete slabs. Structures & Buildings 2001; 146(4): 353-362.
[17] Taylor S.E., Mullin B. Arching action in FRP reinforced concrete slabs. Costruction and Building Materials 2006; 20: 71-80.
[18] Amir S. Compressive Membrane Action in Prestressed Concrete Deck Slabs. ISBN: 978-90-8891-895-7 Printed by: Uitgeverij BOXPress. 2014.
[19] Amir S., Veen V.D., Walraven J. Numerical investigation of the bearing capacity of transversely prestressed concrete deck slab. Proceedings of EURO-C 2014 Conference, 2: 999-1009, Austria 24 -27 March 2014.
[20] Kirkpatrick J., Rankin G., Long A. The influence of compressive membrane action on the serviceability of beam and slab bridge decks. The Struct Eng 1986; 64B(1); 6-12.
[21] Taylor S.E., Rankin G., Cleland D. Real strength of high-permormance concrete bridge deck slabs. Bridge Engineering 2003; 156(BE2): 81-90.
[22] Hewitt B.E., Batchelor B.D. Punching shear strength of restrained slabs. J of the Struct Div 1975; 101(9): 1837-1853.
[23] Bakht B., Csagoly R.P. Bridge testing. Ontario Ministry of Transportation and Communications, Research Report.
[24] (OMTC). Ontario Highway Bridge Design Code. 1979; Highway Engineering Division, 1st edition, Ontario, Canada.
[25] Rankin G.I.B. and Long A.E. Arching action strength enhancement in laterally restrained slab strips. Proc. Instn Civ Engrs Structs & Bldgs, 1997; 122: 461 – 467.
[26] Park R., Gamble W. Reinforced concrete slabs. New York: John Wiley & Sons, 2000, p. 716.
[27] Das S., Morley C. Compressive membrane action in circular reinforced slabs. International Journal of Mechenical Sciences 2005; 47: 1629-1647.
[28] Kirkpatrick, J. , Rankin, G.I.B. and Long, A.E. Strength evaluation of M-beam bridge deck. Structural Engineer, 1984; 62b(3): 60-68.
[29] Belletti B., Damoni C., Hendriks M.A.N., de Boer A. Analytical and numerical evaluation of the design shear resistance of reinforced concrete slabs. Structural Concrete 2014; 15(3): 317-330.
[30] Pimentel M., Figueiras J. Safety assessment of a bridge deck slab using NLFEA and a semi-probabilistic global resistance safety factor. Proceedings of EURO-C 2014 Conference, 2: 1031-1040, Austria 24 -27 March 2014.
[31] Pimentel M., Brühwiler E., Figueiras J. Safety examination of existing concrete structures using the global resistance safety factor concept. Engineering Structures 2014; 70: 130–143.
[32] Belletti B., Vitulli F., Walraven J.C. Compressive membrane action in confined RC and SFRC circular slabs. Proceedings of EURO-C 2014 Conference, 2: 807-818, Austria 24 -27 March 2014.

[33] Belletti B, Esposito R, Walraven JC. Shear capacity of normal, lightweight, and high-strength concrete beams according to ModelCode2010. Part II: experimental results versus nonlinear finite element program results. J Struct Eng 2013;139(12):1600–7.
[34] Taylor R., Maher D.R.H., Hayes B. Effect of the arrangement of reinforcement on the behaviour of reinforced concrete slabs. Magazine of Concrete Research, 1966; 18(55): 85-93.
[35] Belletti B, Bernardi P., Cerioni R., Iori I. Non-linear analysis of reinforced concrete slabs. Proceedings of ISEC 2002 Conference, 1: 663-668, Rome, Italy, 23-26 September 2003.
[36] Belletti B, Meda A., Plizzari G. Design aspects on steel fiber-reinforced concrete pavements. Journal Of Materials In Civil Engineering 2008; 20(9): 599-607.
[37] di Prisco M., Dozio D., Belletti B. On the fracture behaviour of thin-walled SFRC roof elements. Material and Structures 2013; 46(5): 803-829.
[38] Belletti B., Damoni C., Gasperi A. Modeling approaches suitable for pushover analyses of RC structural wall buildings; Engineering Structures 2013, 57: 327-338.
[39] Muttoni A. Punching Shear Strength of Reinforced Concrete Slabs without Transverse Reinforcement. ACI Structural Journal 2008; 105(4): 440-450.
[40] Natário F., Fernández Ruiz M., Muttoni A. Shear strength of RC slabs under concentrated loads near clamped linear supports. Engineering Structures 2014; 76: 10–23.
[41] Koppitz R., Kenel A., Keller T. Effect of punching shear on load–deformation behavior of flat slabs. Engineering Structures 80, 2014: 444–457.
[42] fib Model Code for Concrete Structures 2010. 2013. Wilhelm Ernst & Sohn, Germany.
[43] Belletti B, Cerioni R, Iori I. A Physical Approach for Reinforced Concrete (PARC) membrane elements. J Struct Eng 2001;127(12):1412–26.
[44] Muttoni A., Fernández Ruiz M. The levels-of-approximation approach in MC 2010: application to punching shear provisions. Structural Concrete, 2012; 13(1): 32-41.
[45] Maya D.L.F., Fernández R.M., Muttoni A., Foster S.J. Punching shear strength of steel fibre reinforced concrete slabs. Engineering Structures 2012; 40: 93-94.
[46] Clément, T., Pinho R.A., Fernández R.M., Muttoni, A. Influence of prestressing on the punching strength of post-tensioned slabs. Engineering Structures 2014; 72: 56-69.
[47] Einpaul J., Fernández R.M., Muttoni, A. Influence of moment redistribution and compressive membrane action on punching strength of flat slabs. Engineering Structures, 2015; 86: 43-57
[48] Clément T., Ramos A.P., Fernández Ruiz M., Muttoni A. Design for punching of prestressed concrete slabs. Structural Concrete, Lausanne, Switzerland, 2012.
[49] Belletti B., Pimentel M., Scolari M., Walraven J.. Safety assessment of punching shear failure according to level of approximation approach. Submitted to Structural Concrete, Lausanne, Switzerland.